The Negative Cone Mosaic: A New Manifestation of the Optical Stiles-Crawford Effect in Normal Eyes

Chahira Miloudi,[1,2] Florence Rossant,[3] Isabelle Bloch,[4] Céline Chaumette,[1] Alexandre Leseigneur,[1] José-Alain Sahel,[1] Serge Meimon,[5] Sarah Mrejen,[1] and Michel Paques[1]

[1]Quinze-Vingts Hospital, Departement Hospitalo-Universitaire SightMaintain, Institut National de la Recherche Medicale (INSERM)–Direction de l'Hospitalisation et de l'Organisation des Soins CIC 1423, Paris, France
[2]Alten Corporation, Boulogne Billancourt, France
[3]Institut Supérieur d'Electronique de Paris, Paris, France
[4]Institut Mines Telecom, Telecom ParisTech, Centre National de la Recherche Scientifique Laboratoire Traitement et Communication de l'Information, Paris, France
[5]Office National d'Etudes et de Recherches Aéronautiques, Châtillon, France

PURPOSE. The purpose of this study was to describe a previously unreported manifestation of the optical Stiles-Crawford effect (oSCE) in normal eyes.

METHODS. In a cohort of 50 normal subjects, the directional reflectance of cones in the retinal periphery was explored by flood-illuminated adaptive optics (FIAO) and optical coherence tomography (OCT).

RESULTS. In 32 eyes (64%), off-axis FIAO images of the retinal periphery (~15–20° from the fovea) showed variably sized patches of hyporeflective dots (called here negative mosaic) coexisting with hyperreflective (positive) cones. In nine cases, shifting the entry pupil toward the optical axis restored the positive cone mosaic, with a point-by-point correspondence between positive and negative mosaics. Rods remained hyperreflective around negative and positive cones. These changes were paralleled by changes of the OCT reflectance of the cone outer segment tips and, to a lesser extent, of the inner/outer segment limit.

CONCLUSIONS. By en face FIAO imaging of the retina, the contrast of cones over rods may be strongly dependent on the entry pupil to such an extent that their reflectance is lower than that of rods. We hypothesized that the negative cone mosaic aspect results from the differential Stiles-Crawford effect of cones and rods. Cone reflectance by en face FIAO parallels the reflectance from the cone outer segment tip line and to a lesser extent of the inner/outer segment limit by OCT. Taking this into account, the oSCE is of importance for the interpretation of high-resolution images of photoreceptors. (ClinicalTrials.gov number, NCT01546181.)

Keywords: photoreceptors, adaptive optics, optical coherence tomography, optical Stiles-Crawford effect

Cone photoreceptors have a strong directional selectivity, a property called the Stiles-Crawford effect (SCE). The discovery of a reduced foveal sensitivity when illuminating the fovea off-axis[1,2] revealed the functional importance of the SCE. It was later observed that the reflectance of cones also shows angle-dependent variability, either by reflectometry,[3,4] scanning laser ophthalmoscopy with[5] or without[6,7] adaptive optics, wavefront sensing,[8] or optical coherence tomography (OCT).[9] This gave rise to the concept of optical SCE (oSCE).[10] However, the clinical relevance of oSCE remains poorly known.

While examining the peripheral retina of healthy eyes, we incidentally observed patches of what could be described as negative mosaic, that is, a strong attenuation of the cone reflectance relative to the background giving rise to a contrast inversion. To our knowledge, this has not been previously reported. Here, we explored this feature to verify the hypothesis that it represents a physiologic manifestation of the oSCE.

MATERIALS AND METHODS

Fifty healthy subjects were recruited among controls within an ancillary study of an ongoing study on photoreceptor imaging (registered in ClinicalTrials.gov NCT01546181) for which they gave informed consent. This institutional clinical study was carried out according to the principles outlined in the Declaration of Helsinki. Approval of the ethics committee of the Saint-Antoine hospital (Paris, France) was obtained. The cohort was composed of 28 women and 21 men, with ages ranging from 25 to 66 years and with no ocular medical history. Their mean refraction error was −1.75 diopters (D) (range, −4 to +0.5 D).

Flood-illumination adaptive optics (FIAO) imaging was done with a commercially available FIAO camera (rtx1; Imagine Eyes, Orsay, France). The adaptive optics loop features a 750-nm superluminescent diode beam to measure the point spread function by a Shack-Hartmann wavefront sensor (40 × 32 array). Correction is performed via a deformable mirror (mirao
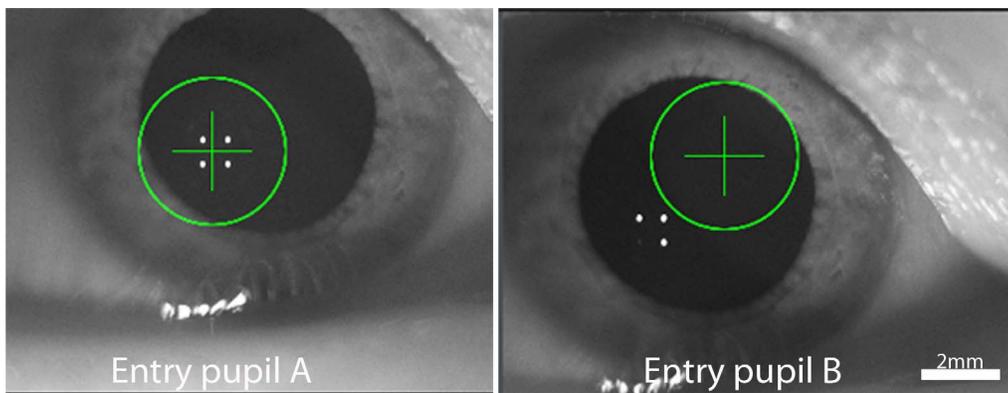
FIGURE 1. Screen capture of the anterior segment image of the viewer interface of the FIAO camera showing the placement of the entry beam (*green cross*) in a right eye gazing superonasally. The *four white dots* are the first Purkinje images indicating the tip of the cornea relative to the frontal plane. In all cases, the negative mosaic was observed close to position A (i.e., close to the inferotemporal rim of the pupil), while the positive mosaic was observed closer to position B (i.e., close to the superonasal rim).

52e; Imagine Eyes). The imaging path is composed of a 850-nm flood illumination beam from a light emitting diode (LED) with a size of 2.5 mm at the pupil illuminating a uniform $4° × 4°$ field on the retina, whose reflection is captured by a $656 × 494$-pixel charge-coupled device.

The fundus imaging procedure is briefly summarized here. En face FIAO fundus images were obtained through fully dilated pupils (1% tropicamide; Novartis, Rueil Malmaison, France) in light-adapted, unbleached eyes. During examination, two live screen images are displayed: one showing the adaptive optics corrected fundus image and the other showing the corneal reflection (first Purkinje image) of four LED sources together with the center of the entry beam (Fig. 1). As the internal fixation target can only explore the posterior pole 10° from the fovea, an external target guiding the fellow eye was required to navigate in the retinal periphery. However, due to the asymmetric configuration of the system, only in the right eye could the periphery be examined. When a negative mosaic

was identified on the live fundus display, an image was acquired coaxially to the corneal reflex (i.e., in the case of a right eye gazing superonasally, close to point A; Fig. 1). Then, the entry pupil was manually shifted as far as possible toward the corneal apex (i.e., close to point B, which is closer to the optical axis), and another image of the same region was acquired. The shift of the entry beam was measured on screen captures of the anterior segment. Although patches of negative mosaics could be identified at similar eccentricities in all directions (data not shown), the data presented thereafter were obtained in the superonasal retina.

Each stack of 40 raw images acquired by the AO camera was processed using the software provided by the manufacturer (CK v0.1; Imagine Eyes).[11] Raw images were registered and averaged to produce a final image with improved signal-to-noise ratio; the background of the resulting image was subtracted using a Gaussian filter, and the histogram was stretched over a 16-bit range of gray levels. The positions of
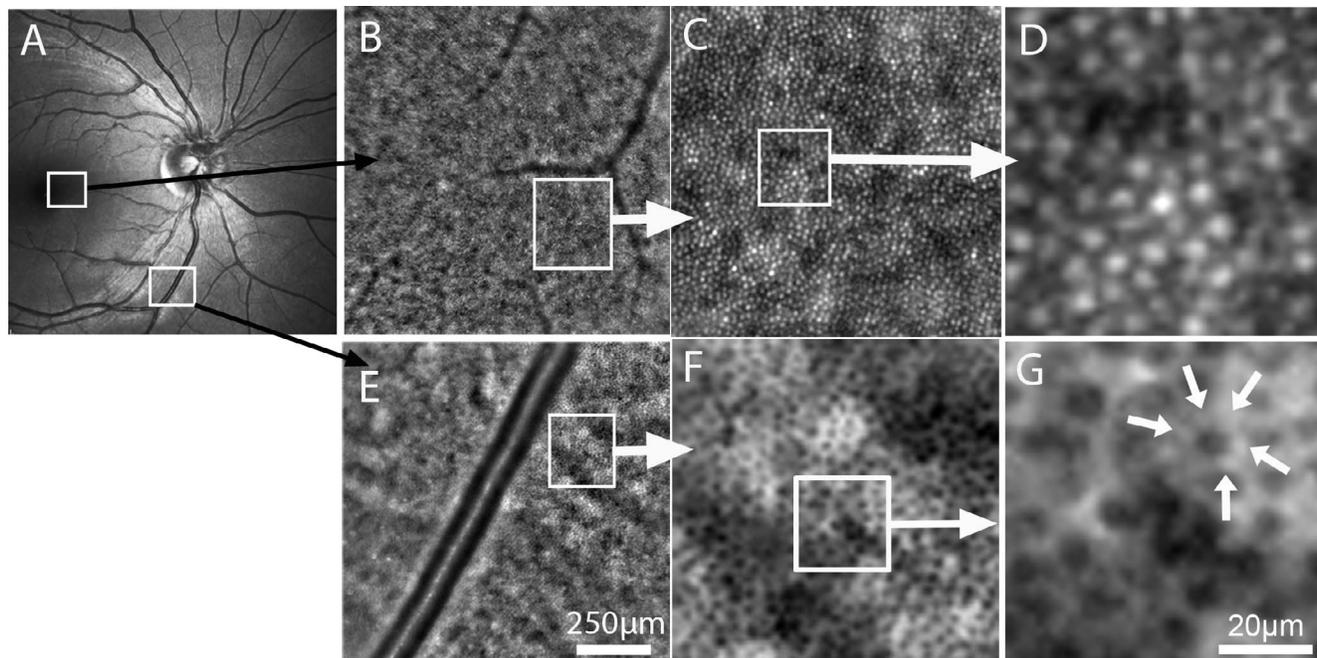
FIGURE 2. Representative AO images of a positive (**B–D**) and negative (**E–G**) cone mosaic in the retina of a normal eye. Note the regular mosaic of small dots, presumably rods, around negative cones (*small arrows* in **G**).
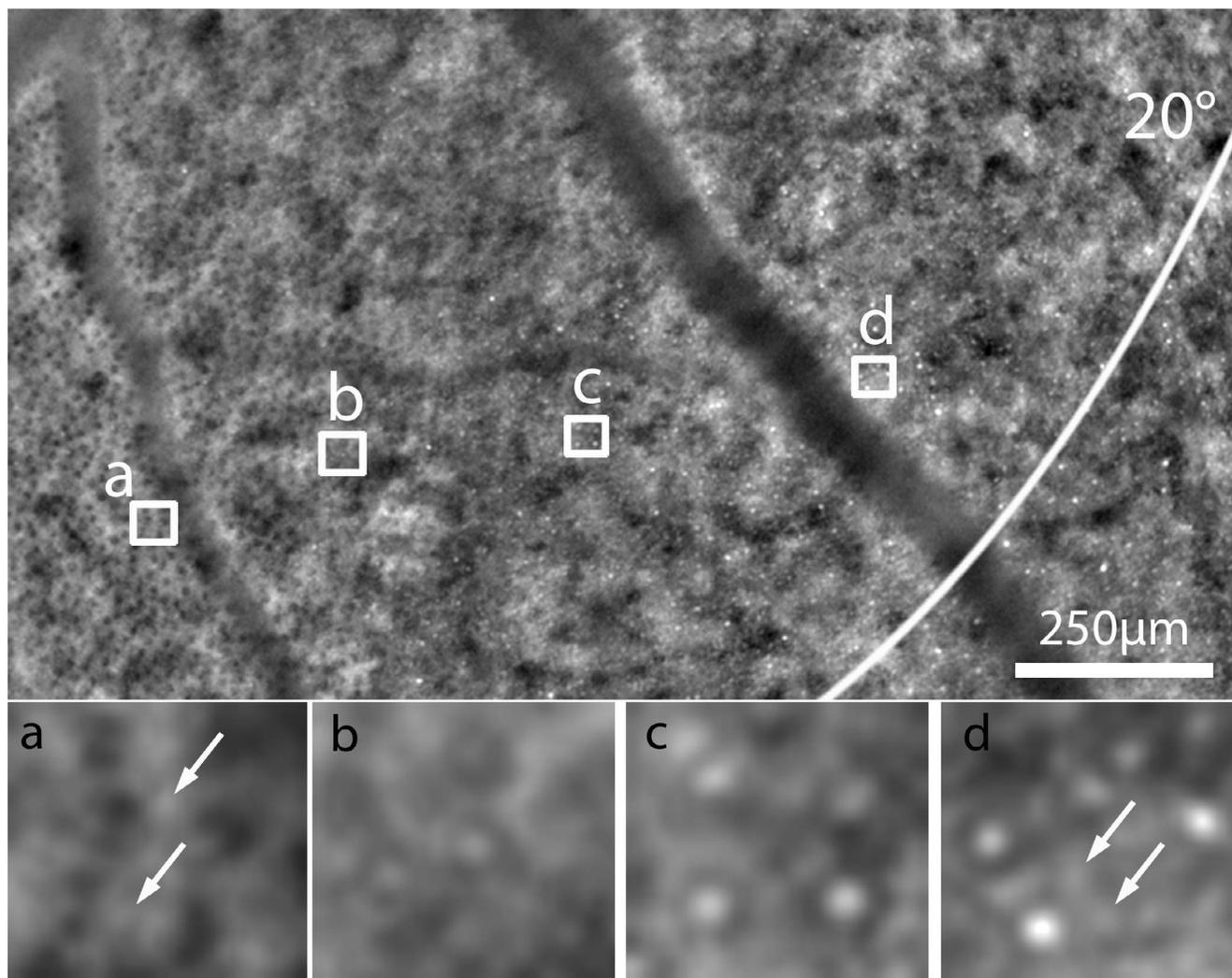
FIGURE 3. Coexistence of negative and positive mosaics within a single FIAO image. The curved line delimits 20° foveal eccentricity. (*Bottom*) Magnifications highlighting the change in cone phenotype from the negative (**a**) to the positive (**d**) mosaic. Note the visibility of rods (*small arrows*) around both negative and positive cones.

photoreceptors in positive mosaics were computed using the software provided by the manufacturer (AOdetect v0.1, Imagine Eyes). For cone counting in negative mosaics, the image was transformed into its negative. Images taken at different entry pupils were registered by rotation and size adjustment using Adobe Photoshop 7.0 (Adobe Corporation, Mountain View, CA, USA).

The OCT was done using a Spectralis scanning laser ophthalmoscope-OCT (Heidelberg Engineering, Heidelberg, Germany). In regions in which negative cones were found, OCT scans through two entry pupil were acquired. As opposed to the FIAO camera, the OCT system does not allow visualizing the entry pupil. Therefore, two entry pupils, one as close as possible to point A and the other one as close as possible to point B, were empirically positioned by taking into account the presumed position of the pupil. In order to limit averaging artifacts, the number of scans to be averaged was fixed at two. The built-in registration procedure ensured automatic registration of OCT scans taken at different entry pupils. Registration was considered acceptable if there were no obvious changes in choroidal patterns between the images. Intensity plots of gray scales of OCT scans were generated using ImageJ (version 1.49; developed by Wayne Rasband; available at http://rsb.info.

nih.gov/ij). Lateral pixels were averaged over 100 μm to minimize the effect of scatter. Plots were rescaled assuming a zero value for the vitreous and normalized to the retinal pigment epithelium (RPE), which was reported to be invariant with light incidence.[9]

RESULTS

In 32 eyes (64%), FIAO imaging at ∼15° to 20° eccentricity showed patches of mosaic of hyporeflective dots (called the negative mosaic; Fig. 2). The mean diameter ± SD of these hyporeflective dots was 6.27 ± 1.1 μm, and their mean density ± SD was 4458 ± 1112/mm². In most cases, within a single image, negative cones coexisted with positive cones (Fig. 3); the area covered by negative cones in a single image varied from 42% to 83% (mean, 61%). Smaller hyperreflective dots, presumably rods, with an apparent diameter in the range of 3 μm, displayed in two to three rows between cones, were seen packed around the hyporeflective dots; their faint contrast with the background did not allow precise measure of their size or density.
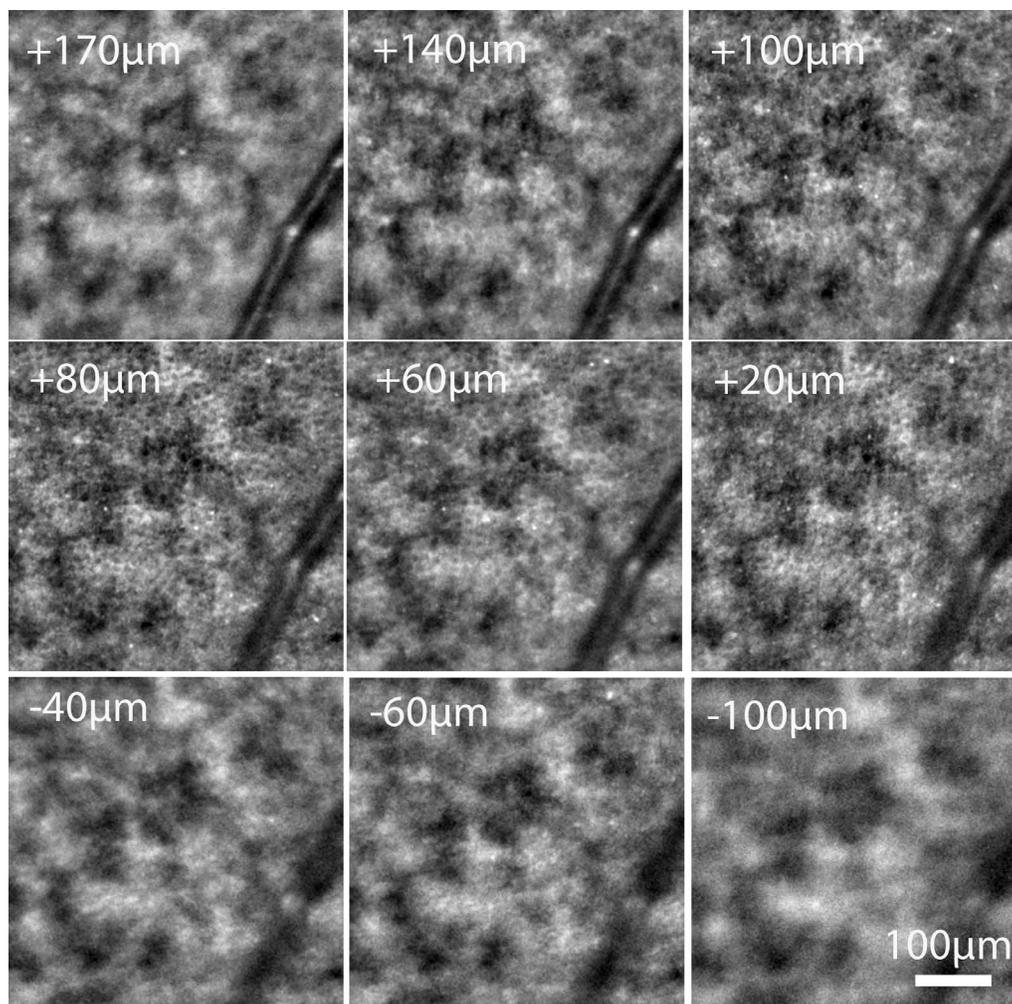
FIGURE 4. Negative cone mosaic observed at different level of focus (indicated in each image), showing that defocusing does not result in a switch to positive mosaic (defocusing of a positive mosaic is shown in Supplementary Fig. S1).

In order to rule out defocus as the cause of the negative mosaic pattern, FIAO images were acquired at different levels of focus in five eyes. Defocus did not lead to a switch positive to negative cones or vice versa (Fig. 4; Supplementary Fig. S1). Negative mosaics were also detected in raw images (Supplementary Fig. S2), ruling out an artifact from image processing.

Shifting the entry pupil from the corneal reflex (point A) to the corneal apex (point B; i.e., closer to the optical axis) attenuated the contrast of the negative mosaic in all eyes. In nine of these eyes (Figs. 5, 6), this even restored the positive cone mosaic. Registration of negative and positive mosaics confirmed that negative and positive mosaics mirrored (Fig. 5). The lateral shift of the entry beam required to observe such a switch from a negative to a positive mosaic ranged from 2.54 to 6.65 mm. The mean density $\pm$ SD of positive cones in areas showing a switch from negative to positive cones ranged from $502 \pm 318/mm^2$ in negative mosaics to $4514 \pm 3498/mm^2$ in positive mosaics. Figure 6 illustrates the variations of cone counts in an area showing a switch from positive to negative cones.

The identification of regions showing a strong directional modulation of the reflectance of cones offered the opportunity to correlate FIAO and OCT imaging by exploring the corresponding changes in the reflectance of the outermost bands by OCT (Figs. 7, 8). In all cases, directional changes in cone reflectance paralleled the directional changes in reflec-

tance of the cone outer segment tip (COST) line and to a lesser extent of the inner/outer segment (IS/OS) limit.

DISCUSSION

Here we report a previously unrecognized manifestation of the oSCE in normal eyes, that is, contrast inversion of the cone mosaic. Registration of negative and positive mosaics suggested indeed that the negative mosaic was a mirror view of the positive cone mosaic. This was not reported in previous studies of high resolution imaging of peripheral retina.[7,12,13]

In all eyes, a mosaic of reflective structures ~3 μm in diameter was consistently present around negative and positive cones. We assumed that this corresponded to the reflection from rods. The transverse resolution of our camera (2.4 μm) indeed theoretically enables to detect peripheral rods, which are larger than rods in the posterior pole.[14,15] The rod/cone distribution found here was similar to that shown by in vivo high-resolution imaging and histology reports.[13] We therefore hypothesize that the reflectance of rods indeed contributed significantly to the reflectance around cones. Switching the entry pupil did not result in obvious changes in the rod reflectance, which is in accordance with the notion that rods have a reduced oSCE compared with cones.[2,10]
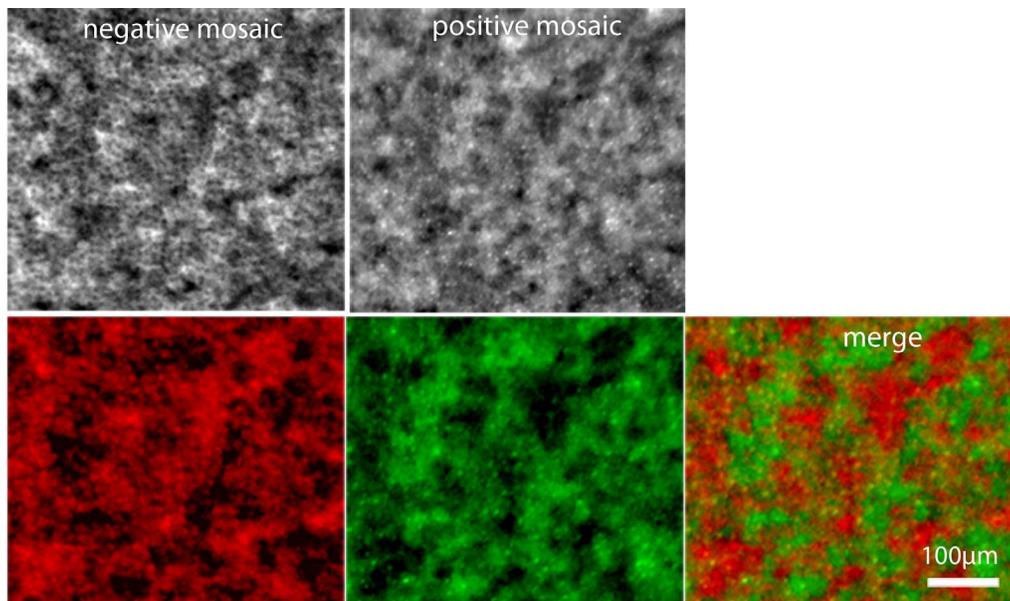
FIGURE 5. Registration of negative and positive mosaics. Negative and negative mosaics (*top row*) of the same retinal area have been color coded (*bottom row*). The negative of the original image of the negative mosaic was color coded in *red* in such a way that hyporeflective cones appear in *bright red*; therefore, in the merged image, cones that have switched from negative to positive are in *yellow*.

Therefore, the negative pattern probably results from the differential oSCE between rods and cones.

A negative cone mosaic was not observed in all eyes, raising the issue about the specificity of eyes with negative mosaics. However, it is of interest to note that as we gained expertise in the use of the camera, we increased the rate of eyes in which a negative mosaic could be found. Crucial points appear to be the obtention of a fully dilated pupil, which maximizes the angulation of incident light with the cones and the careful observation of the fundus on the live image screen. As a result, the last 20 patients that we examined all showed patches of negative mosaic. Hence, we believe that negative mosaics can be observed by this camera in virtually all normal eyes, and hence that it is relatively independent of the biometrics characteristics of the eye.

Negative mosaics were not observed in the macula, but only around 15° to 20° from the fovea. This seemingly contradicts the fact that directional variations of the outer band reflectance
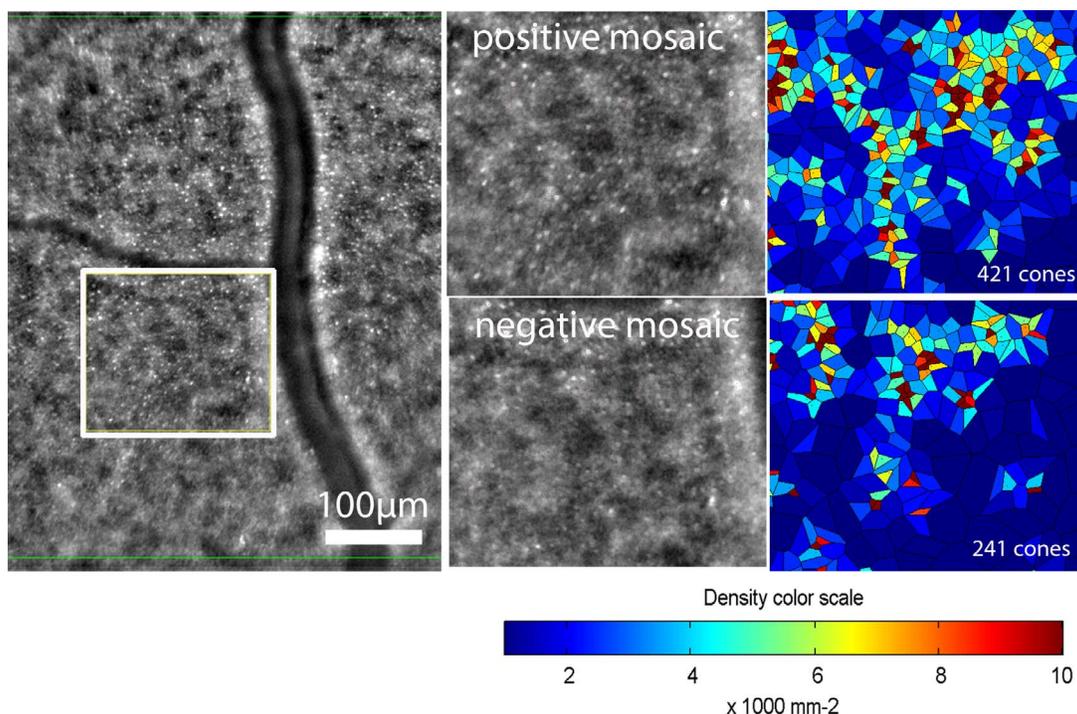
FIGURE 6. Effect of shifting the entry pupil on automated cone counts. In a given retinal region, automated cone counts were done in positive and negative mosaics. The number of detected cones is smaller in the negative cone mosaic.
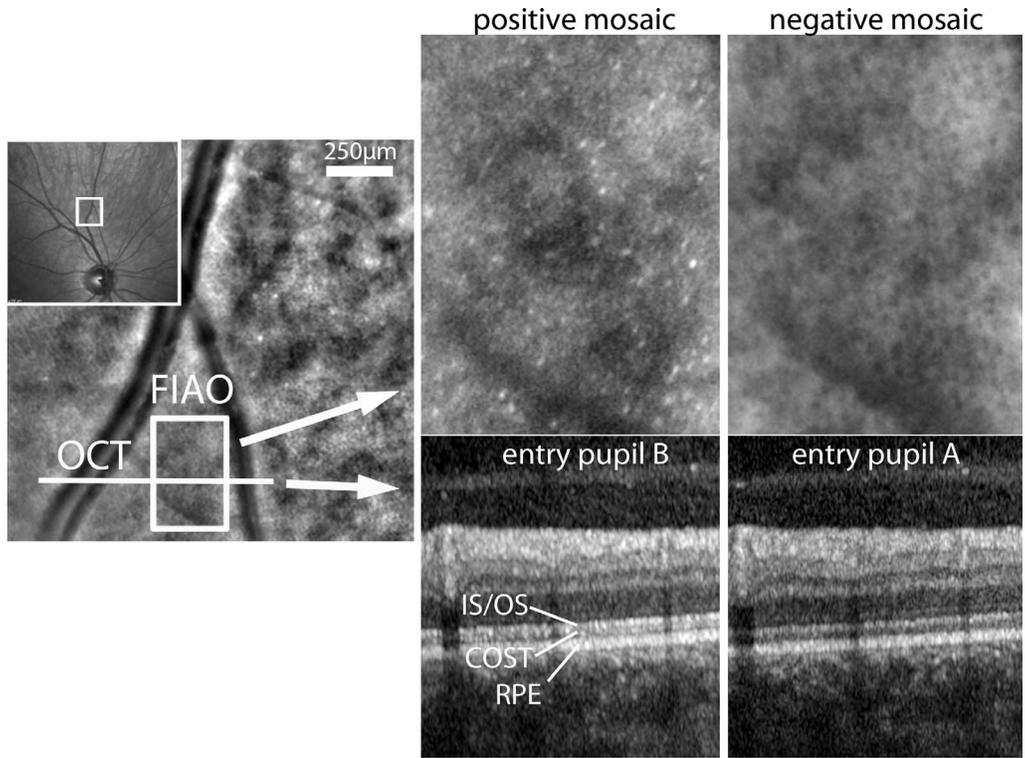
positive mosaic   negative mosaic

FIGURE 7. Directional reflectance of photoreceptors on OCT scans. OCT scans of a retinal region showing negative mosaic were captured through different entry pupils. Note the decreased reflectance of the COST line and of the IS/OS limit in the negative pattern.

by OCT have been already reported in the macula.[9] Although we did not observe negative mosaics in the macula, we cannot exclude that there was indeed directional variability of photoreceptor reflectance on FIAO images of the macula since

we did not measure the absolute reflectance of cones but rather subjectively appreciated the contrast of cones over the background. Assuming that the directional reflectance of individual cones shows a Gaussian profile, it is possible that
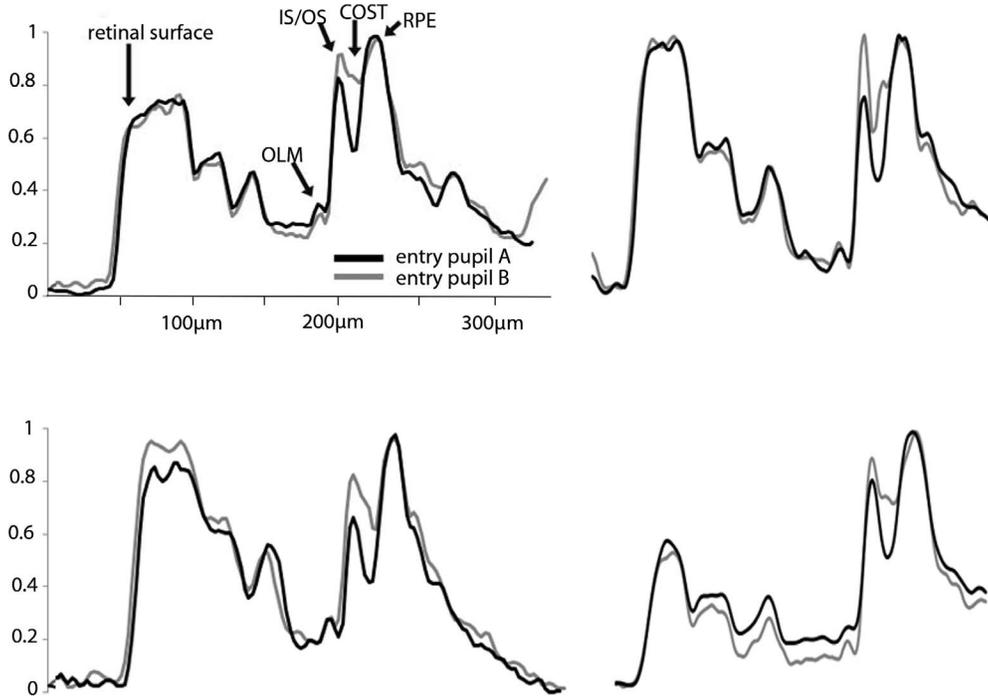
FIGURE 8. Superimposition of intensity plots of gray levels of OCT scans corresponding to positive (*gray lines*) and negative (*black lines*) cone mosaics. Pairs of plots were rescaled assuming a zero value for the vitreous and normalized to the RPE. Note that in all cases the relative decrease of the reflectance of the COST line is more important than that of the IS/OS junction. OLM, outer limiting membrane.

Investigative Ophthalmology & Visual Science

the steeper angle of peripheral cones relative to the plane of the RPE[16] maximized the angulation of cones relative to the incident light, which was then closer to the trough of the Gaussian curve. Alternative explanations would be that peripheral cones show a stronger oSCE and/or that they are misaligned. It has been suggested that the SCE is correlated with the diameter of cones, that is, larger cones show a stronger SCE.[17] Histology studies suggest that cones and rods increase in size from the center to the periphery.[18] Accordingly, the oSCE of foveal cones, which are smaller, is less important than that of parafoveal cones.[4,14] Thus, the negative cone mosaic found in the peripheral retina may be due to a stronger oSCE of larger cones. However, a scanning laser ophthalmoscope (SLO) imaging study found that the oSCE did not significantly vary from 5° to 20° from the fovea.[7] Misalignment of peripheral cones is another possible explanation. An interesting finding was that there was coexistence of negative and positive mosaics in the same 4° image. Psychophysical measures of the SCE in retinal periphery reported a slight, nonsystematic divergence of the alignment of peripheral versus foveal cones,[19] yet the significance of this difference as regard the precision of the measure is unknown.

Combining directional reflectance by OCT and FIAO is potentially of interest to improve our understanding of the oSCE. On OCT scans of normal eyes, at least four parallel hyperreflective bands can be identified at the photoreceptor–RPE interface. Although the anatomical correspondences of these bands are still debated,[20–22] it is generally considered that the second band is at the IS/OS limit. A similar controversy affects the third band, which is attributed to the COST by most authors, although others favor a slightly different hypothesis stating that it corresponds to the interdigitation between the RPE extensions and the cone outer segments.[22] We found that, relative to the RPE, the COST showed more directional variations than the IS/OS. This is rather consistent with histology, since the COST line is cone specific, whereas rods and cones both contribute to the IS/OS line. Our findings are in accordance with a previous study,[9] which has also shown that the outer retinal band showing the most important directional variation is the COST line.

Our study has significant technical limitations. We could not measure the absolute reflectance of cones since the built-in processing of FIAO images includes averaging, Gaussian filtering, and histogram stretching, which unavoidably alters photoreceptor reflectance. Moreover, we limited ourselves to two points in the pupil, which in the case of OCT could not be known with precision. These factors limited the analysis of the correlation between light incidence and reflectance. Also, as our FIAO system is not confocal, focusing may have varied between eyes. An in silico modeling suggested that contrast inversion of cones may results from the specific optical properties of outer segments.[23] Images very similar to negative cones have been obtained in vitro by focusing between the COST and the RPE,[24] probably because of the shorter length of the outer segment of cones. However, in our patients, defocusing did not result in a transition from positive to negative mosaic or vice versa. The large depth of focus of our system relative to the length of the COST may have overcome the distance between the outer segment tips of cone and rods.

Although in the present study we only examined normal eyes, it is likely that these findings may help to refine our interpretations of images from diseased retinas. Indeed, automated cone counts or segmentation algorithms of OCT scans may vary in their result according to the angle of incident light, which is usually not recorded at the time of examination. This effect is probably dependent on the size of the entry pupil. Studies comparing FIAO and OCT in diseased retinas led to the conclusion that the reflectance of the COST line is strongly correlated to the visibility of cones in FIAO images.[25,26] However, even in the presence of convergent findings from en face and OCT imaging, it cannot be concluded for a given subject that cones outer segments are absent in an area showing absence of the COST and of a cone mosaic. Our findings indeed suggest that the decreased intensity of the reflectance of the COST line seen in a particular incidence may be due to misaligned cones. Hence, integrating images from several entry pupils may contribute to disambiguate missing from off-axis cones. Another interesting consequence of our findings is that the presence of directional reflectance may actually be helpful to identify cones within a remodeled retina. Accordingly, it has been shown that extracting the asymmetric component of photoreceptor reflectance (split-detection[27]) is a powerful means for the identification of cones in a dystrophic retina. The Henle fibers,[28–30] the nerve fiber layer,[31] and Gunn's dots[32] also show strong directional reflectance; hence, multiangle imaging appears as a necessary procedure for adequate interpretation of high-resolution retinal imaging.

Acknowledgments

Disclosure: **C. Miloudi**, None; **F. Rossant**, None; **I. Bloch**, None; **C. Chaumette**, None; **A. Leseigneur**, None; **J.-A. Sahel**, None; **S. Meimon**, None; **S. Mrejen**, P; **M. Paques**, Imagine Eyes (C), P

References

1. Stiles WS, Crawford BS. The luminous efficiency of rays entering the eye pupil at different points. *Proc R Soc Lond*. 1933;112:428–450.

2. Flamant F, Stiles WS. The directional and spectral sensitivities of retinal rods to adapting fields of different wavelengths. *J Physiol*. 1948;107:187–202.

3. Gorrand JM, Delori FC. A reflectometric technique for assessing photoreceptor alignment. *Vision Res*. 1995;35:999–1010.

4. Burns SA, Wu S, Delori FC, Eisner AE. Direct measurement of human cone photoreceptor alignment. *J Opt Soc Am A*. 1995;12:2329–2338.

5. Roorda A, Williams DR. Optical fiber properties of individual human cones. *J Vis*. 2002;2:404–412.

6. Delint PJ, Berendschot TM, van Norren D. Local photoreceptor alignment measured with a scanning laser ophthalmoscope. *Vision Res*. 1997;37:243–248.

7. Rativa D, Vohnsen B. Analysis of individual cone-photoreceptor directionality using scanning laser ophthalmoscopy. *Biomed Opt Express*. 2011;2:1423–1431.

8. Gao W, Jonnal RS, Cense B, Kocaoglu OP, Wang Q, Miller DT. Measuring directionality of the retinal reflection with a Shack-Hartmann wavefront sensor. *Opt Express*. 2009;17:23085–23097.

9. Gao W, Cense B, Zhang Y, Jonnal RS, Miller DT. Measuring retinal contributions to the optical Stiles-Crawford effect with optical coherence tomography. *Opt Express*. 2008;16:6486–6501.

10. Westheimer G. Directional sensitivity of the retina: 75 years of Stiles-Crawford effect. *Proc Biol Sci*. 2008;275:2777–2786.

Investigative Ophthalmology & Visual Science

11. Gocho K, Sarda V, Falah S, et al. Adaptive optics imaging of geographic atrophy. *Invest Ophthalmol Vis Sci*. 2013;54: 3673–3680.

12. Merino D, Duncan JL, Tiruveedhula P, Roorda A. Observation of cone and rod photoreceptors in normal subjects and patients using a new generation adaptive optics scanning laser ophthalmoscope. *Biomed Optics Express*. 2011;2:2189–2201.

13. Dubra A, Sulai Y, Norris JL, et al. Noninvasive imaging of the human rod photoreceptor mosaic using a confocal adaptive optics scanning ophthalmoscope. *Biomed Optics Express*. 2011;2:1864–1876.

14. Curcio CA, Sloan KR, Kalina RE, Hendrickson AE. Human photoreceptor topography. *J Comp Neurol*. 1990;292:497–523.

15. Jonas JB, Schneider U, Naumann GO. Count and density of human retinal photoreceptors. *Graefes Arch Clin Exp Ophthalmol*. 1992;230:505–510.

16. Laties AM, Leibman P, Campbell C. Photoreceptor orientation in the primate eye. *Nature*. 1968;218:172–173.

17. Vohnsen B, Iglesias I, Artal P. Guided light and diffraction model of human-eye photoreceptors. *J Opt Soc Am A Opt Image Sci Vis*. 2005;22:2318–2328.

18. Westheimer G. Dependence of the magnitude of the Stiles-Crawford effect on retinal location. *J Physiol*. 1967;192:309–315.

19. Bedell HE. Central and peripheral retinal photoreceptor orientation in amblyopic eyes as assessed by the psychophysical Stiles-Crawford function. *Invest Ophthalmol Vis Sci*. 1980; 19:49–59.

20. Spaide RF, Curcio A. Anatomical correlates to the bands seen in the outer retina by optical coherence tomography: literature review and model. *Retina*. 2011;31:1609–1619.

21. Jonnal RS, Kocaoglu OP, Zawadzki RJ, Lee SH, Werner JS, Miller DT. The cellular origins of the outer retinal bands in optical coherence tomography images. *Invest Ophthalmol Vis Sci*. 2014;55:7904–7918.

22. Staurenghi G, Sadda S, Chakravarthy U, Spaide RF. International Nomenclature for Optical Coherence Tomography (IN•OCT) Panel. Proposed lexicon for anatomic landmarks in normal posterior segment spectral-domain optical coherence tomography: the IN•OCT consensus. *Ophthalmology*. 2014; 121:1572–1578.

23. Vohnsen B. Directional sensitivity of the retina: A layered scattering model of outer-segment photoreceptor pigments. *Biomedical Optics Express*. 2014;5:1569–1587.

24. Packer OS, Williams DR, Bensinger DG. Photopigment transmittance imaging of the primate photoreceptor mosaic. *J Neurosci*. 1996;16:2251–2260.

25. Jacob J, Paques M, Krivosic V, et al. Meaning of visualizing retinal cone mosaic in adaptive optics images. *Am J Ophthalmol*. 2015;159:118–123.

26. Ooto S, Hangai M, Sakamoto A, et al. High-resolution imaging of resolved central serous chorioretinopathy using adaptive optics scanning laser ophthalmoscopy. *Ophthalmology*. 2010; 117:1800–1809.

27. Scoles D, Sulai YN, Langlo CS, et al. In vivo imaging of human cone photoreceptors inner segments. *Invest Ophthalmol Vis Sci*. 2014;55:4244–4251.

28. Lujan BJ, Roorda A, Knighton RW, Carroll J. Revealing Henle's fiber layer using spectral domain optical coherence tomography. *Invest Ophthalmol Vis Sci*. 2011;52:1486–1492.

29. Lujan BJ, Roorda A, Croskrey JA, et al. Directional optical coherence tomography provides accurate outer nuclear layer and Henle fiber layer measurements. *Retina*. 2015;35:1511–1520.

30. Otani T, Yamaguchi Y, Kishi S. Improved visualization of Henle fiber layer by changing the measurement beam angle on optical coherence tomography. *Retina*. 2011;31:497–501.

31. Knighton RW, Huang XR. Directional and spectral reflectance of the rat retinal nerve fiber layer. *Invest Ophthalmol Vis Sci*. 1999;40:639–647.

32. Paques M, Miloudi C, Leseigneur A, Chaumette C, Koch E. High resolution imaging of Gunn's dots. *Retina*. 2015;35:120–124.

Investigative Ophthalmology & Visual Science